Apparent size effects on dopant activation in nanometer-wide Si fins

Folkersma, Steven; Bogdanowicz, Janusz; Favia, Paola; Wouters, Lennaert; Petersen, Dirch Hjorth; Hansen, Ole; Henrichsen, Henrik Hartmann; Nielsen, Peter Former; Shiv, Lior; Vandervorst, Wilfried

Published in:
Journal of Vacuum Science and Technology. Part B. Microelectronics and Nanometer Structures

Link to article, DOI:
10.1116/6.0000921

Publication date:
2021

Document Version
Publisher's PDF, also known as Version of record

JVST B
Journal of Vacuum Science & Technology B

Apparent size effects on dopant activation in nanometer-wide Si fins

Cite as: J. Vac. Sci. Technol. B **39**, 023202 (2021); https://doi.org/10.1116/6.0000921
Submitted: 12 January 2021 . Accepted: 03 March 2021 . Published Online: 23 March 2021

Steven Folkersma, Janusz Bogdanowicz, Paola Favia, Lennaert Wouters, Dirch Hjorth Petersen, Ole Hansen, Henrik Hartmann Henrichsen, Peter Former Nielsen, Lior Shiv, and Wilfried Vandervorst

JVST B
Journal of Vacuum Science & Technology B

ARTICLE

avs.scitation.org/journal/jvb

Apparent size effects on dopant activation in nanometer-wide Si fins

Cite as: J. Vac. Sci. Technol. B 39, 023202 (2021); doi: 10.1116/6.0000921
Submitted: 12 January 2021 · Accepted: 3 March 2021 ·
Published Online: 23 March 2021

Steven Folkersma,[1,2,a)] Janusz Bogdanowicz,[1] Paola Favia,[1] Lennaert Wouters,[1] Dirch Hjorth Petersen,[3] Ole Hansen,[4] Henrik Hartmann Henrichsen,[5] Peter Former Nielsen,[5] Lior Shiv,[5] and Wilfried Vandervorst[1,2]

AFFILIATIONS

[1]IMEC, Kapeldreef 75, B-3001 Leuven, Belgium
[2]Instituut voor Kern-en Stralingsfysika, KU Leuven, Celestijnenlaan 200D, B-3001 Leuven, Belgium
[3]Department of Energy Conversion and Storage, Technical University of Denmark, Fysikvej, Building 310, DK-2800 Kgs Lyngby, Denmark
[4]DTU Nanolab, Technical University of Denmark, Building 347, DK-2800 Kgs Lyngby, Denmark
[5]CAPRES A/S, DTU Science Park, Building 373, DK-2800 Kgs Lyngby, Denmark

[a)]**Electronic mail:** steven.folkersma@imec.be

ABSTRACT

Due to the dramatic downscaling of device features in recent technology nodes, characterizing the electrical properties of these structures is becoming ever more challenging as it often requires metrology able to probe local variations in dopant and carrier concentration with high accuracy. As no existing technique is able to meet all requirements, a correlative metrology approach is generally considered a solution. In this article, we study size-dependent effects on the dopant activation in nanometer-wide Si fins using a novel correlative approach. We start by showing that the micro four-point probe technique can be used to precisely measure the resistance of B doped and (laser) annealed Si fins. Next, we use transmission electron microscopy and scanning spreading resistance microscopy to show that the observed width dependence of the apparent sheet resistance of these fins can be explained by either a partially or a fully inactive region forming along the top of the fin sidewalls according to the annealing conditions.

I. INTRODUCTION

Since the introduction of nanoscale device structures such as the fin field-effect transistor,[1] metrology aimed at the electrical characterization of such features is facing unprecedented challenges.[2] Indeed, characterizing the electrical properties of these features, which can be impacted by their nanoscale dimensions via, e.g., size-dependent dopant activation, diffusion, and recrystallization,[3–5] often requires metrology that is able to probe variations in dopant/carrier concentration within a few nanometers and with high accuracy.[2,6] For example, while a width-dependent sheet resistance has been observed in B-implanted Si fins using the micro four-point probe (μ4PP)[7–10] technique, this technique alone is not sufficient to characterize the (local) electrical properties of these structures. Additionally, scanning spreading resistance microscopy (SSRM)[2,11,12] measurements are difficult to quantify for such nanometer scaled features, as the measured spreading resistance is easily impacted by parasitic series resistances.[13] As such, a correlative approach, i.e., combining the information obtained with different techniques, is generally proposed as a solution to collect reliable information on the (size-dependent) electrical properties of these nanoscale objects.[14,15]

In this article, we propose a novel correlative approach to study apparent size-dependent dopant activation in nanometer-wide B doped Si fins. In this approach, we combine the structural information acquired with transmission electron microscopy (TEM) with the electrical information obtained with both SSRM and μ4PP. Using the latter two electrical analysis techniques allows one to exploit both the high lateral resolution (<1 nm^2) of SSRM with the incomparable accuracy (~1%[7,9,10,16]) and speed of μ4PP.

We start by showing that the apparent sheet resistance of the B doped Si fins, as measured by μ4PP, rapidly increases as fins become narrower than 100 nm in width. Second, we use a correlative study including TEM and SSRM to show that the observed

increase in apparent sheet resistance is actually explained by either a nonconductive (i.e., inactive) amorphous region or a less conductive defective region along the top of the fin sidewalls, depending on the annealing condition, while the dopant activation (and thus sheet resistance) away from the fin sidewalls remains constant as a function of fin width.

II. EXPERIMENT

In order to study the apparent size effects on the dopant activation in Si fins, we use three different test structures each consisting of B-implanted (3×10^{15} cm^{-2}, 5 kV, 7° tilt, four-sided implant at room temperature) Si fins with fin widths (W_{fin}) ranging between ~450 and ~20 nm.[8] The B was implanted after filling the space between the ~300 nm tall fins with shallow trench isolation oxide. The electrical isolation from the substrate was ensured by implantation of a deep lowly n-doped well.[17] For each of the three test structures, a different annealing condition was used, i.e., (1) a 450 °C oven anneal for 15 s, (2) a 1150 °C millisecond laser anneal with three scans, and (3) a 1250 °C millisecond laser anneal with three scans.[18]

The fin resistance of the B-implanted Si fins was measured using the μ4PP technique, which has been demonstrated to be capable of precisely measuring the resistance of nanometer-wide fins with high precision ($\sigma < 3\%$).[9,10] The inset of Fig. 1 shows a schematic of the μ4PP electrodes landed on a B-implanted Si fin. The electrical resistance of the portion of the fin between the two inner electrodes (i.e., R_{fin}), is then measured by injecting a current I_{in} into the sample with the two outer electrodes while measuring the induced voltage drop V using the inner two electrodes such that $R_{fin} = V/I_{in}$. For the measurements in this article, we use a modulated current I_{in} with an amplitude of 1 μA and a frequency of 49 Hz. For our samples, R_{fin} is obtained for the different fin widths by scanning the μ4PP electrodes across the fin arrays with a step size ranging between ~200 and 50 nm, depending on the fin pitch. W_{fin} was extracted using TEM for the <100 nm wide fins and scanning electron microscopy for the >100 nm wide fins.

III. DISCUSSION

Figure 1(a) shows the value of the measured R_{fin} for fins of the same width W_{fin} and the three different annealing conditions. As can be seen, R_{fin} expectedly increases with decreasing fin width and with decreasing annealing temperature.[18] Moreover, the values measured in Fig. 1(a) are in agreement with values measured before on the same structures with similar B-implanting and annealing conditions.[9,10] For a fin doped and activated uniformly along its width, R_{fin} can be obtained from[9]

$$R_{fin} = R_S \times d/W_{fin}, \quad (1)$$

where $d = 8\,\mu$m [i.e., the distance between the μ4PP electrodes, see the inset of Fig. 1(a)] and R_S is the sheet resistance of the activated profile in the fin. The dashed lines of Fig. 1(a) were obtained using Eq. (1) assuming $R_S = R_S^{pad}$, i.e., considering an identical doping and activation in the fins as in an $80 \times 80\,\mu m^2$ pad, which underwent the same implant and annealing conditions. As can be observed, the experimental data points are in good agreement with the obtained dashed lines for fins down to ~100 nm in width, indicating that the electrical properties of the material inside these fins and in the pad are fairly close and that the change in resistance as

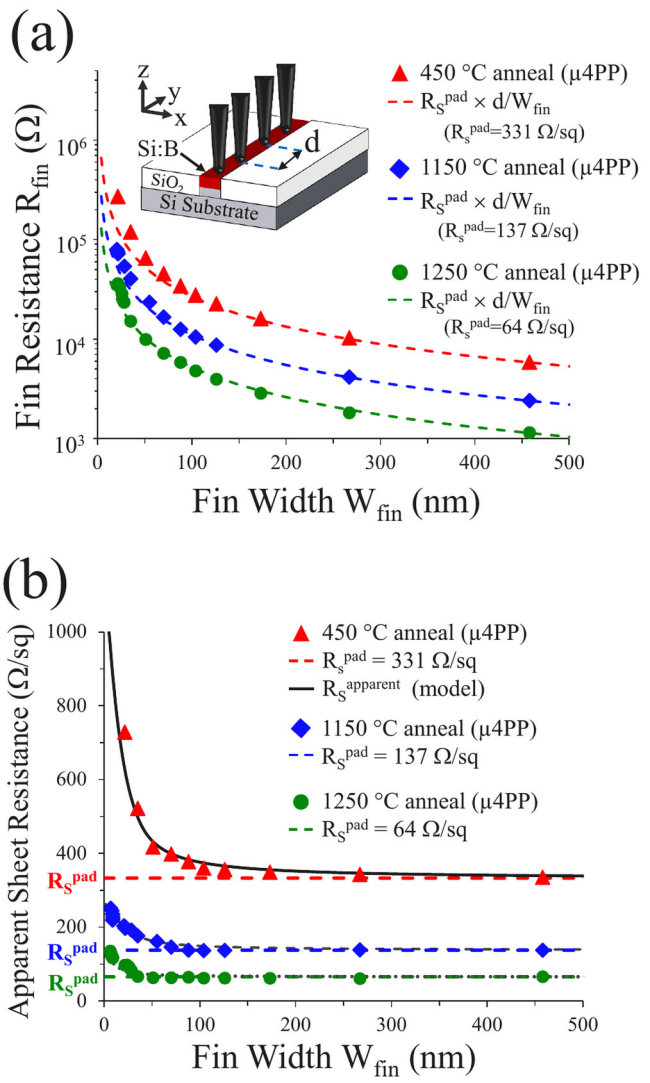

FIG. 1. (a) Fin resistance R_{fin} measured by μ4PP for Si fins with varying widths, implanted with B (3×10^{15} cm^{-2}, 5 keV) and annealed with a 450 °C oven anneal (triangles), a 1150 °C laser anneal (diamonds), or a 1250 °C laser anneal (circles). The dashed lines correspond to the resistance calculated using $R = R_S^{pad} \times d/W_{fin}$, where R_S^{pad} is the sheet resistance measured in a large pad which received the same implant and annealing steps. (inset) Schematic of the four μ4PP electrodes, spaced a distance d apart, landed on a B-implanted Si fin where the fin resistance is measured by $R_{fin} = V/I_{in}$. (b) Apparent fin sheet resistance extracted from the data in Fig. 1(a), which shows a rapid increase for fins <100 nm in width. The R_S^{pad} for the corresponding annealing conditions (dashed lines) and the apparent fin sheet resistance calculated from the conductivity model (black lines) discussed in Fig. 2 are also shown.

a function of fin width is mostly due to geometrical confinement as modeled by Eq. (1). However, for the narrow (i.e., $W_{fin} < 100$ nm) fins, the measured resistance appears to increase (see especially the 450 °C anneal case) with respect to the obtained dashed lines.

To evaluate the impact of the fin dimensions on the electrical properties more precisely for these narrow ($W_{fin} < 100$ nm) fins, it is useful to define an apparent sheet resistance by inverting Eq. (1) such that

$$R_S^{apparent} = R_{fin} \times W_{fin}/d. \quad (2)$$

Figure 1(b) shows $R_S^{apparent}$ as obtained from Eq. (2) using the measured R_{fin} shown in Fig. 1(a). Interestingly, $R_S^{apparent}$ monotonically increases for fins below 100 nm in width for all three annealing schemes. It can be understood that this increase is linked to a drop in electrical conductivity as the fin shrinks. Unfortunately, μ4PP alone cannot determine whether this is due to a uniform drop in conductivity in the fin or rather a local deactivation of the dopants. Indeed, the μ4PP technique is sensitive to the integral of the conductivity distribution $\sigma(x, z)$ across the fin cross section, i.e., $R_{fin} = \frac{1}{\iint(x, z)\, dx\, dz} \times d$ [see the inset of Fig. 1(a) for x and z directions][19] or for the measured apparent sheet resistance,

$$R_S^{apparent} = \frac{W_{fin}}{\iint(x, z)\, dx\, dz}. \quad (3)$$

In order to get more insight into the conductivity distribution $\sigma(x, z)$, we conduct a correlative study including TEM and SSRM. As can be seen in Figs. 2(a)–2(c), for the case of the low temperature 450 °C anneal, an amorphous region along the top of the fin sidewalls can be observed by TEM [Figs. 2(a)–2(c), white arrows].[20] The SSRM measurement on the same 35 nm wide fin structure shown in Fig. 2(b) shows that this amorphous region is ~4 orders of magnitude more resistive (~10^8 Ω, see the green region at the top of the fin sidewall) as compared to the resistance measured away from the fin sidewall [~10^4 Ω, see the red region in Fig. 2(d)].

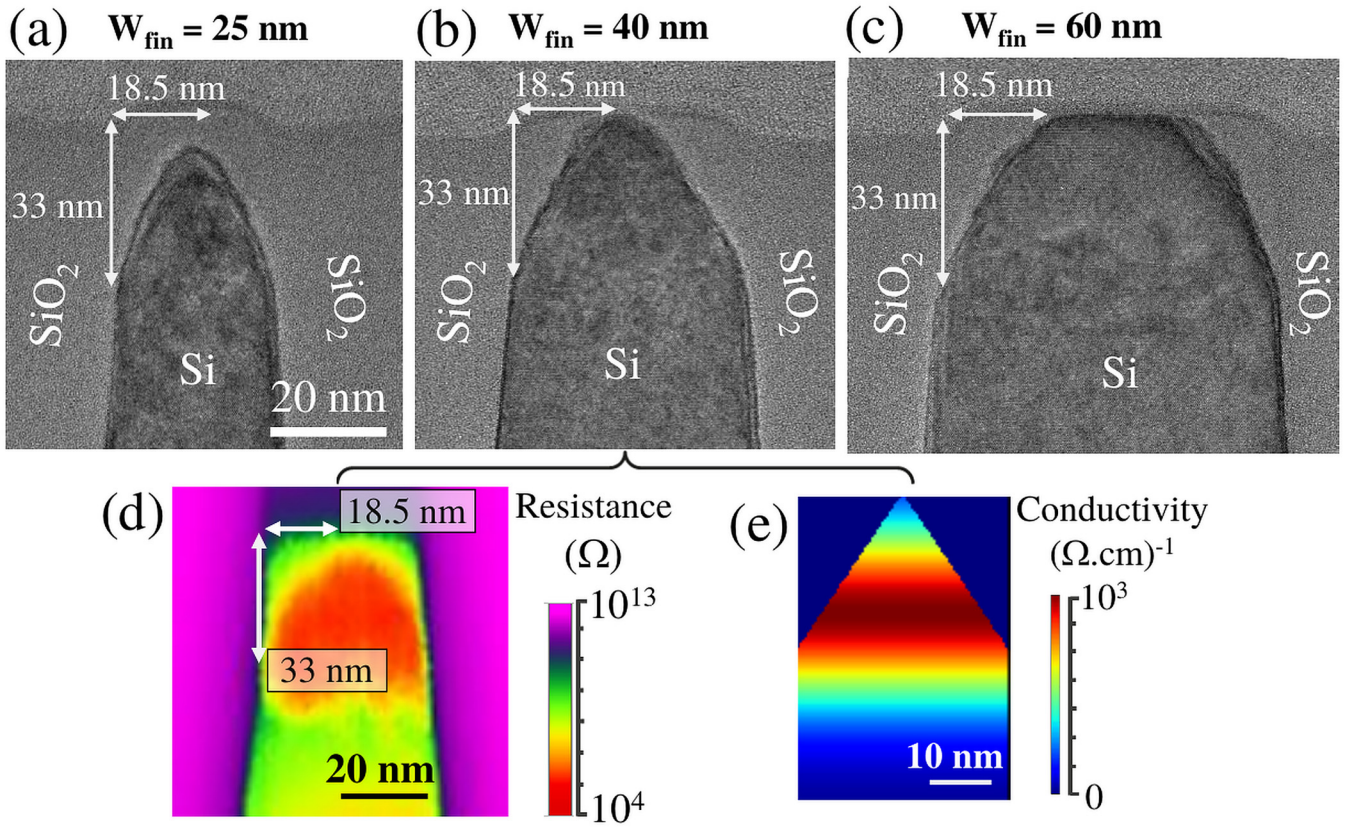

FIG. 2. (a)–(c) TEM image of a 20 (a), 35 (b), and 55 nm (c) wide B-implanted Si fin embedded in SiO_2, showing the remaining implant damage (i.e., amorphous Si) along the top of the fin sidewalls (white arrows) after a 450 °C anneal. The white arrows show the average size (±0.5 nm) of this region measured for the different fin widths, indicating that the size is constant. (d) SSRM image showing that the amorphous area observed in Fig. 2(b) is indeed highly resistive (white arrows). Indeed, the size of this region is similar to the size of the amorphous region observed in Fig. 2(b). (e) Schematic of our conductivity model for a 35 nm wide fin in the case of the 450 °C anneal based on the TEM image in Fig. 2(b).

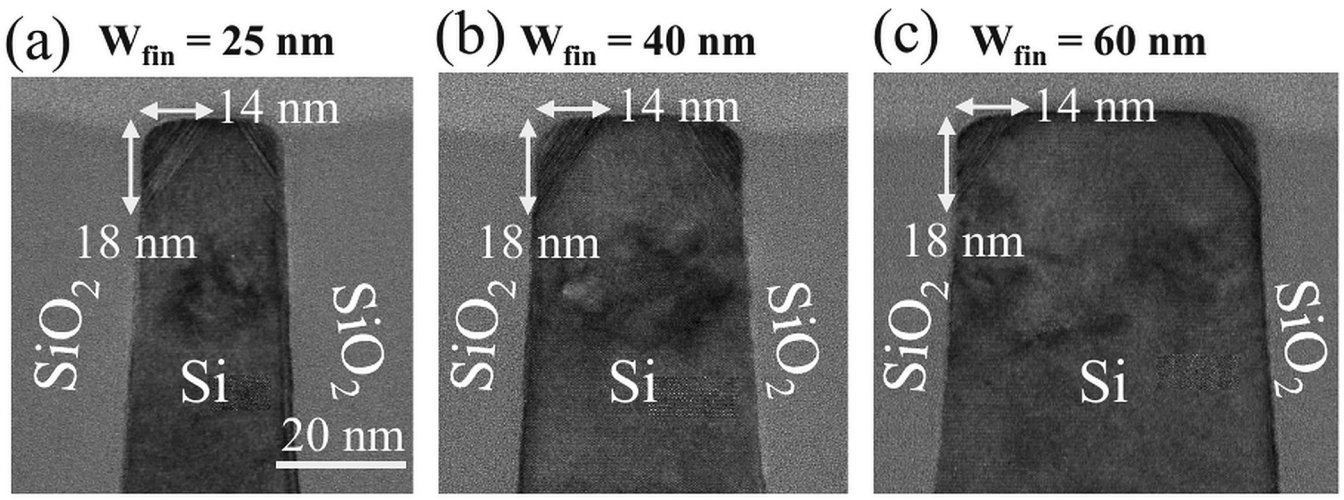

FIG. 3. (a)–(c) TEM image of a 20-nm (a), 35-nm (b), and 55-nm (c) wide B-implanted Si fin embedded in SiO_2, showing the remaining (111) defects along the top of the fin sidewalls (white arrows) after a 1150 °C laser anneal. The white arrows show the average size (±0.5 nm) of this region measured for the different fin widths, indicating that the size is constant.

Moreover, this amorphous region remains constant in size as a function of fin width [see Figs. 2(a)–2(c)], i.e., its relative contribution to the cross section increases. Hence, this explains the monotonic increase in $R_S^{apparent}$ observed in Fig. 1(b) for decreasing fin widths.

To quantify the increase in $R_S^{apparent}$, we propose a simple model for the cross-sectional conductivity profile inside the fin [see an example of $W_{fin} = 35$ nm in Fig. 2(e)] based on the TEM images in Figs. 2(a)–2(c). For this model, we first determine the conductivity profile of the active region of the fin, i.e., $\sigma_{active}(x,z)$. To do this, we start by calculating the as-implanted B depth profile using Stopping and Range of Ions in Matter (SRIM) calculations[21] for the same implanting conditions used for the Si fins. Next, a 15% dopant activation is assumed, such that, by calculating the corresponding conductivity profile assuming crystalline mobilities, the resulting sheet resistance matches the sheet resistance measured in a large pad (i.e., $R_S^{pad} = 331\ \Omega/sq$) for the 450 °C anneal case. Note that a concentration-independent dopant activation, as is used here, was indeed observed in Si fins with similar B implant and anneal conditions.[22] Next, we consider the amorphous region as nonconductive (i.e., inactive) such that $\sigma_{amorphous}(x,z) = 0$. The constant size of the nonconductive region in Fig. 2(e) corresponds to the size of the amorphous region observed in TEM [see white arrows in Figs. 2(a)–2(c)]. This model is then used to calculate the apparent sheet resistance for all fin widths using Eq. (3). As shown by the theoretical black line in Fig. 1(b), the conductivity model is in excellent agreement with the measured data for the 450 °C anneal case. This confirms that the increase in apparent sheet resistance as a function of fin width observed for this case can be accurately explained by the existence of the highly resistive amorphous region along the fin sidewalls, while the dopant activation (and thus sheet resistance) away from the fin sidewalls remains constant.

Next, the increase in $R_S^{apparent}$ observed for the smallest fins in the case of the high temperature 1150 °C [see diamonds, Fig. 1(b)] laser anneal can be explained in a similar way by (111) defects still present after laser annealing,[20] as is also observed by TEM [Figs. 3(a)–3(c), white arrows]. Similar to the amorphous Si region observed in the case of a low 450 °C anneal, we can observe a defective area along the top of the fin sidewall, which remains constant in size as a function of fin width [see white arrows, Figs. 3(a)–3(c)]. Unfortunately, we do not know the conductivity of this region, which is very difficult to quantify precisely using SSRM. However, the width dependence of $R_S^{apparent}$ observed in Fig. 1(b) is a measure for the conductivity (i.e., $\sigma_{defective}$) of this region, and we can use the model in Fig. 2(e) to give a rough estimate of this conductivity. Indeed, the apparent sheet resistance calculated for the 1150 °C anneal case using the model in Fig. 2(e), where σ_{active} is now determined using $R_S^{pad} = 137\ \Omega/sq$, is too high (not shown) compared to the measured $R_S^{apparent}$ in Fig. 1(b) for the smallest (<100 nm wide) fins, indicating a degraded conductivity (i.e., $0 < \sigma_{defective} < \sigma_{active}$) in the defected region rather than the zero conductivity of the amorphous region in the 450 °C anneal case. Moreover, by fitting the apparent sheet resistance calculated using Eq. (3) (Fig. 1, dashed black lines) to the measured apparent sheet resistance with μ4PP, the defective area is estimated to be 40% less conductive compared to the Si away from the fin sidewalls (i.e., $\sigma_{defective} = 0.6\ \sigma_{active}$). For the case of the 1250 °C laser anneal (TEM not shown), a similar defective area at the top of the fin sidewalls is observed. Here, using the same method as was used for the 1150 °C anneal case, this defective area is estimated to be 20% less conductive (i.e., $\sigma_{defective} = 0.8\ \sigma_{active}$). Interestingly, combining the apparent sheet resistance extracted with μ4PP with the model in Fig. 2(e) opens up the possibility to study the conductivity of the defected region in the 1150 and 1250 °C laser anneal cases with other techniques.

IV. CONCLUSIONS

In conclusion, we examined apparent size effects on the dopant activation in nanometer-wide B-implanted Si fins. First, we showed that the μ4PP technique can be used to precisely measure (standard deviation <3%) the resistance of B-implanted and (laser-) annealed Si fins. Next, we showed that the observed width dependence of the apparent sheet resistance is explained by either a partially or a fully inactive region forming along the top of the fin sidewalls, depending on the annealing conditions, while the dopant activation (and thus sheet resistance) away from the fin sidewalls remains constant.

DATA AVAILABILITY

The data that support the findings of this study are available from the corresponding author upon reasonable request

REFERENCES

[1]Chenming Hu *et al.*, IEEE Trans. Electron Devices **47**, 2320 (2000).
[2]W. Vandervorst, C. Fleischmann, J. Bogdanowicz, A. Franquet, U. Celano, K. Paredis, and A. Budrevich, Mater. Sci. Semicond. Process. **62**, 31 (2017).
[3]A. Schulze, A. Florakis, T. Hantschel, P. Eyben, A. S. Verhulst, R. Rooyackers, A. Vandooren, and W. Vandervorst, Appl. Phys. Lett. **102**, 052108 (2013).
[4]M. T. Björk, H. Schmid, J. Knoch, H. Riel, and W. Riess, Nat. Nanotechnol. **4**, 103 (2009).
[5]A. Veloso, A. De Keersgieter, P. Matagne, N. Horiguchi, and N. Collaert, Mater. Sci. Semicond. Process. **62**, 2 (2017).
[6]P. Zeitzoff, K. Akarvardar, J. Mody, and A. Konar, *2017 International Conference on Frontiers of Characterization and Metrology for Nanoelectronics* (FCMN, Monterey, CA, 2017), pp. 31–33.
[7]D. H. Petersen, O. Hansen, R. Lin, P. F. Nielsen, T. Clarysse, J. Goossens, E. Rosseel, and W. Vandervorst, *16th IEEE International Conference on Advanced Thermal Processing of Semiconductors (RTP 2008), 2008* (IEEE, New York, 2008), p. 251.
[8]D. H. Petersen, "Micro four-point probe and micro hall effect: Methods for reliable electrical characterization of ultra-shallow junctions," Ph.D. Dissertation, Technical University of Denmark, 2009.
[9]J. Bogdanowicz *et al.*, Phys. Status Solidi Appl. Mater. Sci. **215**, 4 (2018).
[10]S. Folkersma *et al.*, Beilstein J. Nanotechnol. **9**, 1863 (2018).
[11]A. Schulze, T. Hantschel, A. Dathe, P. Eyben, X. Ke, and W. Vandervorst, Nanotechnology **23**, 305707 (2012).
[12]P. De Wolf, J. Snauwaert, T. Clarysse, W. Vandervorst, and L. Hellemans, Appl. Phys. Lett. **66**, 1530 (1995).
[13]K. Pandey, K. Paredis, A. J. Robson, and W. Vandervorst, J. Appl. Phys. **128**, 034303 (2020).
[14]A. Vaid *et al.*, in *Metrology, Inspection, and Process Control for Microlithography XXV* (International Society for Optics and Photonics, Bellingham, WA, 2011), Vol. 7971, p. 797103.
[15]J. Foucher, N. G. S. Figueiro, J. Rouxel, and R. Thérèse, Proc. SPIE **8378**, 83780F (2012).
[16]F. Wang, D. H. Petersen, F. W. Osterberg, and O. Hansen, in *17th International Conference on Advanced Thermal Processing of Semiconductors* (IEEE, New York, 2009), pp. 1–6.
[17]J. Mitard *et al.*, *2014 Symposium on VLSI Circuits* (IEEE, New York, 2014), p. 110.
[18]E. Rosseel, *et al.*, *16th IEEE International Conference on Advanced Thermal Processing of Semiconductors (RTP 2008), 2008* (IEEE, New York, 2008),
p. 135.
[19]D. K. Schroder, in *Semiconductor Material and Device Characterization*, edited by D. K. Schroder (John Wiley & Sons, Inc., Hoboken, NJ, 2005).
[20]R. Duffy, M. J. H. Van Dal, B. J. Pawlak, M. Kaiser, R. G. R. Weemaes, B. Degroote, E. Kunnen, and E. Altamirano, Appl. Phys. Lett. **90**, 241912 (2007).
[21]J. F. Ziegler and J. Biersack, in *Treatise on Heavy-Ion Science*, 6th ed., edited by D. A. Bromley, 6th ed. (Springer Science+Business Media, New York, 1985).
[22]S. Folkersma *et al.*, *Proceedings of International Conference on Ion Implantation Technology, September 2018* (IEEE, Würzburg, Germany, 2018), p. 153.